Research Article GUJ Sci 36(4): 1700-1720 (2023) DOI: 10.35378/gujs.998265

Gazi University

Journal of Science

http://dergipark.gov.tr/gujs

Analytical Modeling of Buckling of Carbon Nanotubes Reinforced Sandwich-Structured Composite Shells Resting on Elastic Foundations

Abdelaziz TIMESLI*

Hassan II University of Casablanca, National Higher School of Arts and Crafts (ENSAM CASABLANCA), AICSE Laboratory, 20670 Casablanca, Morocco.

Highlights

- Analytical models are utilized to study the buckling behavior of CNT reinforced sandwich shells.
- Determination of composite material properties by the rule of mixtures.
- The proposed model can be used to study the effects of various parameters.

Article Info

Received: 21 Sep 2021
Accepted: 14 Dec 2022

Keywords

Stability analysis
Reinforced composite
Sandwich-structured
Elastic foundation
Thin shell theory

Abstract

Sandwich-Structured Composites (SSCs) are widely used in lightweight construction, especially in the aerospace sector, due to their high specific stiffness and strength. Therefore, it is important to develop their quality by using new techniques. Today, nanotechnologies offer new perspectives for the reinforcement of construction materials. This paper assumes that the reinforcement of the sandwich shell is performed by CNT reinforced face sheets with a uniform or Functionally Graded (FG) distribution of CNTs. The effective properties of the Carbon Nanotubes Reinforced Sandwich-Structured Composite (CNT-RSSC) shells are calculated using the rule of mixture. This study presents novel exact analytical formulas to predict the critical buckling load of the CNT-RSSC shells resting on elastic foundations based on Donnell cylindrical shell theory. These analytical formulas provide the most meaningful answer because we get an equation showing us exactly what happens with each variable. The effects of various parameters on the buckling stability of the RSSC shells are examined.

1. INTRODUCTION

Thin shell structures are used in several branches of engineering (aeronautics, spacecraft, aircraft, civil engineering, nuclear reactor, etc.). Reducing the weight and cost of structures is the goal of engineers by using advanced technologies and materials. Advanced nanocomposites materials have become essential in various industrial fields. The nanocomposite materials are treated by many authors to study the dynamic [1-3], static [4, 5] and buckling behavior [6] using different theories of frames, beams, plates and shells [7-13]. In recent years, a new class of CNT reinforced materials has gained more and more attention [14-20]. In these materials, the distributions of CNTs in the structure thickness are considered as uniform or FG. The FG distribution is smooth and continuous throughout the thickness of the structure [21, 22].

In the area of structural engineering, shells are efficient of carrying loads acting perpendicular to their surfaces. It's due to the spatial curvature of the geometry of shells. Spherical and cylindrical shells are often used as elements in such structures. Other structural forms such as beams and plates are structurally less efficient of carrying loads acting on their surfaces by bending action. However, the complex geometry of shells leads to complexities to predict or understand the structural behavior. Thin shell structures, made of new materials and various shapes and geometries, are economical and suitable structural elements for applications in aerospace, aircraft, transportation systems, marine, etc. Among these structures, researchers are interested to the sandwich-structural nanocomposites due to its outstanding properties, which give humanity a superior material [1, 23]. Therefore, carbon fibers, graphene sheets or CNTs are frequently used for the reinforcement of nanocomposite structures. CNTs is discovered in 1991 by Iijima (1991) [24] who

*e-mail: ABDELAZIZ.TIMESLI@univh2c.ma, abdelaziz.timesli@gmail.com

works with NEC Corporation in Japan. For new composites technology using polymer, rubber, metal and epoxy matrices, CNTs are considered the best materials for reinforcement. In the following I provide some researches on reinforced composite structures. Shen (2009) [25] and Shen and Zhang (2010) [26] studied the thermal buckling, nonlinear bending and post-buckling behavior of FG CNT Reinforced (FGCNT-R) composite plates. Sofiyev (2019) [27] investigated the stability of FGCNT-R composite conical shells. Mirzaei and Kiani (2015) [28] analyzed the thermal behavior of FGCNT-R composite conical shells. Kolahchi et al. (2016) [29] and Hajmohammad et al. (2018) [30] investigated flat and cylindrical shells shells reinforced with graphene and CNT. Tagrara et al. (2015) [31] analysed the bending, buckling and free vibration of FGCNT-R composite beams resting on an elastic foundation using a trigonometric refined beam theory, which is developed by the authors. Kaci et al. (2012) [32] investigated the nonlinear bending of FGCNT-R nanocomposite plates under the simultaneous effects of a uniform pressure loading and a thermal environment. In what follows, I discuss some work on elastic foundations. Zaitoun et al. (2022) [33] studied the buckling behavior of a FG sandwich plate embedded on a viscoelastic foundation and subjectyed to hygrothermal conditions. Mudhaffar et al. (2021) [34] used a simple integral Higher-order Shear Deformation Theory (HSDT) to study the bending response of an advanced FG ceramic-metal structure embedded in a viscoelastic foundation and exposed to a hygro-thermo-mechanical load. Merazka et al. (2121) [35] investigated the hygro-thermo-mechanical bending behaviors of simply supported FG plate embedded in a Winkler-Pasternak elastic foundation. Guellil et al. (2021) [36] exposed the bending analysis of FG plates embedded in Pasternak foundation using HSDT. The effect of various types of boundary conditions is investigated.

To improve the compressive strengths and high tensile in components of modern aircraft, CNT-RSSC with two face sheets components are used. For this kind of structures, Wang et al. (2018) [37] studied the vibration analysis of SSC using a new polynomial refined plate theory for the core layer and a classical plate theory for the CNT-R nanocomposite face sheets. Safaei et al. (2018) [38] and Safaei et al. (2019) [39] analyzed the sandwich plates embedded in an elastic foundation and made of an isotropic core layer and two symmetrical nanocomposite face sheets. The authors studied the forced vibration, free vibration, dynamic response and steady state thermal of these plates. Using the same plates configuration as in [38, 39], Mehar et al. (2017) [40] presented the nonlinear eigen frequency response of FGCNT-R sandwich plates. Medani et al. (2019) [41] presented the mechanical response of FGCNT-R porous sandwich polymer plate using the First order Shear Deformation Theory (FSDT). They studied two types of sandwich plates. Firstly, the face sheets are reinforced and the core is homogeneous. Secondly, the face sheets are homogeneous and the core is reinforced.

This research focuses on buckling of CNT-RSSC shells resting on an elastic foundation. The equilibrium equations are developed according to certain assumptions based on the Kirchhoff-Love kinematic. Applying the adjacent equilibrium criterion, I can establish the linearized stability equations to study the onset of buckling. The results show that the CNT distribution, geometrical parameters, thickness ratio of the face sheet to the core, and elastic foundation parameters are factors that affect buckling of the FGCNT-RSSC shells.

2. BASIC FORMULATION

2.1. Kinematic and Constitutive Relations

The SSC shell is assumed to consist of a homogeneous core layer and two surface sheets constructed of CNT-R nanocomposites. The assigned coordinate system and the geometrical characteristics of the spherical shell are described in Figure 1-(a). The SSC spherical shell is symmetric in mid-plane with curved edges a and b and a constant radius of curvature $R = \mathrm{R}_1 + \mathrm{R}_2$. As shown in Figure 1-(b) the thickness of the face sheets is $\mathrm{h_f}$ and that of the homogeneous core is $\mathrm{h_c}$, so that the total thickness of the SSC shell $h = \mathrm{h_c} + 2\mathrm{h_f}$. Cartesian coordinate system is attached to a corner of the mid-surface of the shell where $0 \leq x \leq a$, $0 \leq y \leq b$ and $-0.5h \leq z \leq 0.5h$ through the length, width, and thickness, respectively. The thin shell theory used in this work provides accurate results by considering the assumption of large aspect ratios $\frac{H}{a} \ll 1$ and $\frac{H}{b} \ll 1$ [42-45].

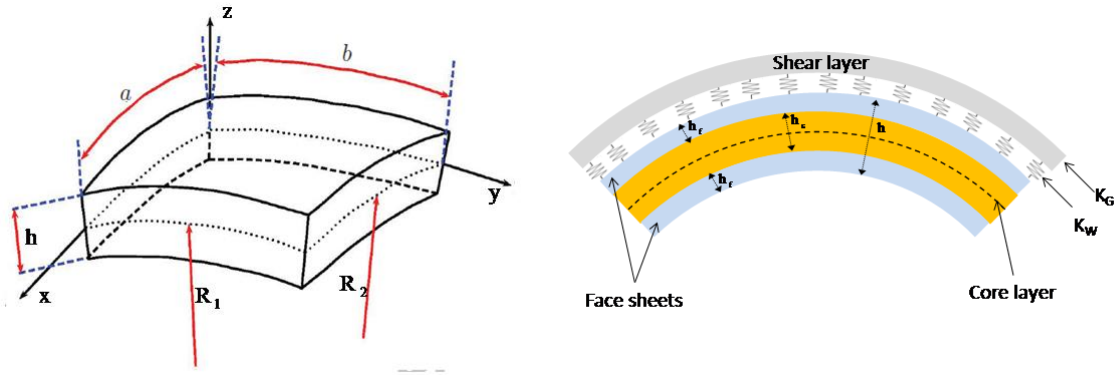

(a) : Configuration and coordinate system of CNT-RSSC shell

(b) : Cross-section of CNT-RSSC embedded in an elastic foundation

Figure 1. *Coordinate system and configuration of CNT-RSSC shell resting on an elastic foundation*

In this research, the estimation of the shell kinematics, as a function of the change in curvature and mid-surface characteristics, is based on the FSDT. Under the assumption of the Kirchhoff-Love hypothesis, the displacement field is given by:

$$\begin{cases} u_x(x,y,z) = u(x,y) - z\dfrac{\partial w}{\partial x} \\ u_y(x,y,z) = v(x,y) - z\dfrac{\partial w}{\partial y} \\ u_z(x,y,z) = w(x,y) \end{cases} \tag{1}$$

where u_x, u_y and u_z are displacement components, u, v and w are displacement components of the mid-surface.

According to the classical thin shell theory, the transverse shear strain is neglected and the in-plane strain components are given as:

$$\begin{Bmatrix} \varepsilon_{xx} \\ \varepsilon_{yy} \\ \gamma_{xy} \end{Bmatrix} = \begin{Bmatrix} \dfrac{\partial u}{\partial x} - \dfrac{w}{R_2} \\ \dfrac{\partial v}{\partial x} - \dfrac{w}{R_1} \\ \dfrac{\partial u}{\partial y} + \dfrac{\partial v}{\partial x} \end{Bmatrix} - z \begin{Bmatrix} \dfrac{\partial^2 w}{\partial x^2} \\ \dfrac{\partial^2 w}{\partial y^2} \\ 2\dfrac{\partial^2 w}{\partial xy} \end{Bmatrix} \tag{2}$$

Under the plane-stress conditions and elastic deformations of the CNT-RSSC shell, the constitutive law of the shell is given in the form:

$$\{\sigma\} = \begin{Bmatrix} \sigma_{xx} \\ \sigma_{yy} \\ \tau_{xy} \end{Bmatrix} = \begin{bmatrix} Q_{11} & Q_{12} & 0 \\ Q_{12} & Q_{22} & 0 \\ 0 & 0 & Q_{66} \end{bmatrix} \begin{Bmatrix} \varepsilon_{xx} \\ \varepsilon_{yy} \\ \gamma_{xy} \end{Bmatrix} \tag{3}$$

where $Q_{ij}(i,j = 1,2,6)$ are the stiffness coefficients of the material which are obtained as Jam and Kiani (2015) [46] and Timesli (2020) [6]:

$$Q_{11} = \frac{E_{11}}{1-\nu_{12}\nu_{21}},\ Q_{22} = \frac{E_{22}}{1-\nu_{12}\nu_{21}},\ Q_{12} = \frac{\nu_{21}E_{11}}{1-\nu_{12}\nu_{21}},\ Q_{66}=G_{12} \tag{4}$$

where E_{ii} are the Young moduli, G_{12} is the shear modulus, and ν_{ij} are the Poisson's ratios.

2.2. CNT Distribution Through the Face Sheet Thickness

Suppose that the distribution of CNTs across the face sheets of SSC is uniform or FG [47]. I designate the uniform distribution by UD and the four functionally graded distributions by FG-X, FG-O, FG-A and FG-V. I consider that the two face sheets of the sandwich shell are made of the same CNTs distribution profiles, as shown in Figure 2.

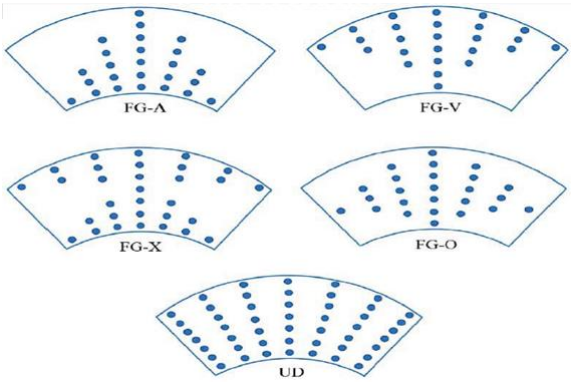

Figure 2. *Different CNTs distributions profiles*

The mathematical forms of the CNT distribution along the face sheet thickness are expressed as follows [6, 21, 22]:

- UD :

$$D_{CN} = D_{CN}^{*} \tag{5}$$

- FG-O:

$$D_{CN} = 2\left(1 - \frac{2|z|}{h}\right) D_{CN}^{*} \tag{6}$$

- FG-X:

$$D_{CN} = 4\frac{|z|}{h} D_{CN}^{*} \tag{7}$$

- FG-V:

$$D_{CN} = \left(1 + \frac{2|z|}{h}\right) D_{CN}^{*} \tag{8}$$

- FG-A:

$$D_{CN} = \left(1 - \frac{2|z|}{h}\right) D_{CN}^{*}. \tag{9}$$

The volume fraction D_{CN}^{*} can be obtained from the following expression:

$$D_{CN}^{*} = \frac{m_{CN}}{m_{CN} + \left(\frac{\rho_{CN}}{\rho_m}\right)(1 - m_{CN})} \tag{10}$$

where ρ_m is the mass density of the matrix, and ρ_{CNT} and m_{CN} are respectively the mass density and mass fraction of CNTs, respectively.

The mechanical properties E_{11}, E_{22}, G_{12} and ν_{12} of nanocomposite face sheets are determined by the following formulas [48]:

$$\begin{cases} E_{11} = \eta_1 D_{CN} E_{11}^{CN} + (1 - D_{CN}) E^m \\ E_{22} = \eta_2 \Big/ \left(\dfrac{D_{CN}}{E_{22}^{CN}} + \dfrac{(1 - D_{CN})}{E_m} \right) \\ G_{12} = \eta_3 \Big/ \left(\dfrac{D_{CN}}{G_{12}^{CN}} + \dfrac{(1 - D_{CN})}{G^m} \right) \\ \nu_{12} = D_{CN}^{*} \nu_{12}^{CN} + (1 - D_{CN}) \nu^m \end{cases} \tag{11}$$

where E^m, G^m and ν^m are material properties of PMMA polymer matrix, E_{11}^{CN}, E_{22}^{CN}, G_{12}^{CN} and ν_{12}^{CN} are material properties of CNTs, η_1, η_2 and η_3 are the corrective parameters [25-26].

2.3. Equilibrium Equations of CNT-RSSC Shell

Using Hamiltons' principle [49], it is possible to derive the equations for static equilibrium of CNT-RSSC shell as follows:

$$\int_{t_1}^{t_2} \delta(U + V) dt = 0 \tag{12}$$

with

$$\delta U = \int_{\omega} \int_{-\frac{h}{2}}^{\frac{h}{2}} \left(\sigma_{xx} \delta \varepsilon_{xx} + \sigma_{yy} \delta \varepsilon_{yy} + \tau_{xy} \delta \gamma_{xy} \right) dz d\omega \tag{13}$$

$$\delta V = \int_{\omega} \int_{-\frac{h}{2}}^{\frac{h}{2}} \left(-f \delta w + N_{xx} \frac{\partial w}{\partial x} \frac{\partial \delta w}{\partial x} + N_{yy} \frac{\partial w}{\partial y} \frac{\partial \delta w}{\partial x} + N_{xy} \frac{\partial w}{\partial x} \frac{\partial \delta w}{\partial y} + N_{xy} \frac{\partial w}{\partial y} \frac{\partial \delta w}{\partial x} \right) d\omega \tag{14}$$

where δU and δV are the variations of the virtual strain energy and the work associated to the displacement field and the external load, respectively, f is the total pressure applied by the elastic foundation and N_{xx}, N_{yy} and N_{xy} are in-plane distributed forces, where N_{xx} and N_{yy} are the normal forces, and N_{xy} is the shear force. The term δU can be rewrite in the following form:

$$\delta U = \int_{\omega} \left(N_{xx} \delta \varepsilon_{xx} + N_{yy} \delta \varepsilon_{yy} + N_{xy} \delta \gamma_{xy} + M_{xx} \delta k_{xx} + M_{yy} \delta k_{yy} + M_{xy} \delta k_{xy} \right) d\omega \, . \tag{15}$$

M_{xx} and M_{yy} are the bending moments and M_{xy} is the twisting moment. Using the Equation (2), the expression of δU becomes:

$$\delta U = \int_{\omega} \left(N_{xx}\delta u_{,x} - \frac{N_{xx}}{R_2}\delta w + N_{yy}\delta v_{,y} - \frac{N_{yy}}{R_1}\delta w + N_{xy}\delta u_{,y} + N_{xy}\delta v_{,x} + M_{xx}\delta w_{,xx} + M_{yy}\delta w_{,yy} + M_{xy}\delta w_{,yx} \right) d\omega \,. \tag{16}$$

Integrating by part of the Equations (17) and (15) gives:

$$\delta U = \int_{\omega} \left(-\frac{\partial N_{xx}}{\partial x}\delta u - \frac{N_{xx}}{R_2}\delta w - \frac{\partial N_{yy}}{\partial y}\delta v - \frac{N_{yy}}{R_1}\delta w - \frac{\partial N_{xy}}{\partial y}\delta u - \frac{\partial N_{xy}}{\partial x}\delta v - \frac{\partial^2 M_{xx}}{\partial x^2}\delta w - \frac{\partial^2 M_{yy}}{\partial y^2}\delta w - 2\frac{\partial^2 M_{xy}}{\partial x \partial y}\delta w \right) d\omega \tag{17}$$

$$\delta V = \int_{\omega} \left(-f + N_{xx}\frac{\partial^2 w}{\partial x^2} + 2N_{xy}\frac{\partial^2 w}{\partial x \partial y} + N_{yy}\frac{\partial^2 w}{\partial y^2} \right) \delta w d\omega \,. \tag{18}$$

Arranging the Equation (18) according to displacements terms (δu, δv, δw), I obtain:

$$\delta U = \int_{\omega} \left(-\left(\frac{\partial N_{xx}}{\partial x} + \frac{\partial N_{xy}}{\partial y}\right)\delta u - \left(\frac{\partial N_{yy}}{\partial y} + \frac{\partial N_{xy}}{\partial x}\right)\delta v - \left(\frac{\partial^2 M_{xx}}{\partial x^2} + 2\frac{\partial^2 M_{xy}}{\partial x \partial y} + \frac{\partial^2 M_{yy}}{\partial y^2} + \frac{N_{xx}}{R_2} + \frac{N_{yy}}{R_1}\right)\delta w \right) d\omega \,. \tag{19}$$

By substitution the Equations (18) and (19) in the Hamilton's principle (12), I obtain the following equilibrium equations:

$$\begin{cases} \delta u: \ \dfrac{\partial N_{xx}}{\partial x} + \dfrac{\partial N_{xy}}{\partial y} = 0 \\ \delta v: \ \dfrac{\partial N_{yy}}{\partial y} + \dfrac{\partial N_{xy}}{\partial x} = 0 \\ \delta w: \ \dfrac{\partial^2 M_{xx}}{\partial x^2} + 2\dfrac{\partial^2 M_{xy}}{\partial x \partial y} + \dfrac{\partial^2 M_{yy}}{\partial y^2} + \dfrac{N_{xx}}{R_2} + \dfrac{N_{yy}}{R_1} + N_{xx}\dfrac{\partial^2 w}{\partial x^2} + 2N_{xy}\dfrac{\partial^2 w}{\partial x \partial y} + N_{yy}\dfrac{\partial^2 w}{\partial y^2} - f = 0 \end{cases} . \tag{20}$$

The constitutive relations of shell are given as follows:

$$\begin{cases} M_{xx} = -D_{11}\dfrac{\partial^2 w}{\partial x^2} - D_{12}\dfrac{\partial^2 w}{\partial y^2} \\ M_{yy} = -D_{12}\dfrac{\partial^2 w}{\partial x^2} - D_{22}\dfrac{\partial^2 w}{\partial y^2} \\ M_{xy} = -2D_{66}\dfrac{\partial^2 w}{\partial x \partial y} \end{cases} , \tag{21}$$

where the bending stiffness coefficients D_{ij} are given by:

$$
\begin{cases}
D_{11} = \int_{-\frac{h}{2}}^{-\frac{h_c}{2}} z^2 \frac{E_{11}(z)}{(1-\nu_{12}(z)\nu_{21}(z))}dz + \int_{-\frac{h_c}{2}}^{\frac{h_c}{2}} z^2 \frac{E^m}{(1-(\nu^m)^2)}dz + \int_{-\frac{h}{2}}^{\frac{h}{2}} z^2 \frac{E_{11}(z)}{(1-\nu_{12}(z)\nu_{21}(z))}dz \\
\quad = \int_{-\frac{h}{2}}^{-\frac{h_c}{2}} z^2 \frac{E_{11}(z)}{(1-\nu_{12}(z)\nu_{21}(z))}dz + \frac{E^m h_c^3}{12(1-(\nu^m)^2)} + \int_{-\frac{h}{2}}^{\frac{h}{2}} z^2 \frac{E_{11}(z)}{(1-\nu_{12}(z)\nu_{21}(z))}dz \\
D_{22} = \int_{-\frac{h}{2}}^{-\frac{h_c}{2}} z^2 \frac{E_{22}(z)}{(1-\nu_{12}(z)\nu_{21}(z))}dz + \int_{-\frac{h_c}{2}}^{\frac{h_c}{2}} z^2 \frac{E^m}{(1-(\nu^m)^2)}dz + \int_{-\frac{h}{2}}^{\frac{h}{2}} z^2 \frac{E_{22}(z)}{(1-\nu_{12}(z)\nu_{21}(z))}dz \\
\quad = \int_{-\frac{h}{2}}^{-\frac{h_c}{2}} z^2 \frac{E_{22}(z)}{(1-\nu_{12}(z)\nu_{21}(z))}dz + \frac{E^m h_c^3}{12(1-(\nu^m)^2)} + \int_{-\frac{h}{2}}^{\frac{h}{2}} z^2 \frac{E_{22}(z)}{(1-\nu_{12}(z)\nu_{21}(z))}dz \\
D_{12} = \int_{-\frac{h}{2}}^{-\frac{h_c}{2}} z^2 \frac{\nu_{21}(z)E_{11}(z)}{(1-\nu_{12}(z)\nu_{21}(z))}dz + \int_{-\frac{h_c}{2}}^{\frac{h_c}{2}} z^2 \frac{\nu^m E^m}{(1-(\nu^m)^2)}dz + \int_{-\frac{h}{2}}^{\frac{h}{2}} z^2 \frac{\nu_{21}(z)E_{11}(z)}{(1-\nu_{12}(z)\nu_{21}(z))}dz \\
\quad = \int_{-\frac{h}{2}}^{-\frac{h_c}{2}} z^2 \frac{\nu_{21}(z)E_{11}(z)}{(1-\nu_{12}(z)\nu_{21}(z))}dz + \frac{\nu^m E^m h_c^3}{12(1-(\nu^m)^2)} + \int_{-\frac{h}{2}}^{\frac{h}{2}} z^2 \frac{\nu_{21}(z)E_{11}(z)}{(1-\nu_{12}(z)\nu_{21}(z))}dz \\
D_{66} = \int_{-\frac{h}{2}}^{-\frac{h_c}{2}} z^2 G_{12}(z)dz + \int_{-\frac{h_c}{2}}^{\frac{h_c}{2}} z^2 G^m dz + \int_{-\frac{h}{2}}^{\frac{h}{2}} z^2 G_{12}(z)dz \\
\quad = \int_{-\frac{h}{2}}^{-\frac{h_c}{2}} z^2 G_{12}(z)dz + \frac{G^m h_c^3}{12} + \int_{-\frac{h}{2}}^{\frac{h}{2}} z^2 G_{12}(z)dz.
\end{cases}
\tag{22}
$$

Replacing the bending stiffness coefficients D_{ij} in the third equation of the system (20) and I obtain:

$$
-D_{11}\frac{\partial^4 w}{\partial x^4} - 2(D_{12}+2D_{66})\frac{\partial^4 w}{\partial x^2 \partial y^2} - D_{22}\frac{\partial^4 w}{\partial y^4} + \frac{N_{xx}}{R_2} + \frac{N_{yy}}{R_1} + N_{xx}\frac{\partial^2 w}{\partial x^2} + 2N_{xy}\frac{\partial^2 w}{\partial x \partial y} + N_{yy}\frac{\partial^2 w}{\partial y^2} - f = 0\,. \tag{23}
$$

The membrane forces can be connected to the stress function ϕ and I can write them as follows:

$$
N_{xx} = \frac{\partial^2 \phi}{\partial y^2}, N_{yy} = \frac{\partial^2 \phi}{\partial x^2} \; and \; N_{xy} = -\frac{\partial^2 \phi}{\partial x \partial y}\,. \tag{24}
$$

The adjacent equilibrium criterion [45, 43, 50] is used to study the possible existence of adjacent equilibrium configurations. I consider that the indices 0 and b represent the quantities pre-buckling and post-buckling, respectively, and we neglect the second order terms in index b to show the equilibrium equation:

$$-D_{11}\frac{\partial^4 w_b}{\partial x^4}-2(D_{12}+2D_{66})\frac{\partial^4 w_b}{\partial x^2\partial y^2}-D_{22}\frac{\partial^4 w_b}{\partial y^4}+\frac{1}{R_2}\frac{\partial^2\phi}{\partial \mathrm{y}^2}+\frac{1}{R_1}\frac{\partial^2\phi}{\partial \mathrm{x}^2}+N_{xx0}\frac{\partial^2 w_b}{\partial x^2}+N_{xy0}\frac{\partial^2 w_b}{\partial x\partial y}+N_{yy0}\frac{\partial^2 w_b}{\partial y^2}-f_b=0\,. \tag{25}$$

The compatibility condition of a shell is given by:

$$\frac{\partial^2\varepsilon_{xx}}{\partial y^2}+\frac{\partial^2\varepsilon_{yy}}{\partial x^2}-\frac{\partial^2\gamma_{xy}}{\partial xy}+\frac{1}{R_1}\frac{\partial^2 w}{\partial x^2}+\frac{1}{R_2}\frac{\partial^2 w}{\partial y^2}=0 \tag{26}$$

The membrane strains are given by:

$$\begin{cases}\varepsilon_{xx}=C_{22}^{*}N_{xx}+C_{12}^{*}N_{yy}\\ \varepsilon_{yy}=C_{12}^{*}N_{xx}+C_{11}^{*}N_{yy}\\ \gamma_{xy}=C_{66}^{*}N_{xy}\end{cases} \tag{27}$$

where

$$\begin{cases}C_{11}^{*}=\dfrac{C_{11}}{\Delta}\\ C_{22}^{*}=\dfrac{C_{22}}{\Delta}\\ C_{12}^{*}=-\dfrac{C_{12}}{\Delta}\\ C_{66}^{*}=\dfrac{1}{C_{66}}\\ \Delta=C_{11}C_{22}-C_{12}^{2}\end{cases} \tag{28}$$

where C_{ij} are the extensional stiffness coefficients of the shell which are given by:

$$
\begin{cases}
C_{11} = \int_{-\frac{h}{2}}^{-\frac{h_c}{2}} \frac{E_{11}(z)}{(1-\nu_{12}(z)\nu_{21}(z))}dz + \int_{-\frac{h_c}{2}}^{\frac{h_c}{2}} \frac{E^m}{(1-(\nu^m)^2)}dz + \int_{-\frac{h}{2}}^{\frac{h}{2}} \frac{E_{11}(z)}{(1-\nu_{12}(z)\nu_{21}(z))}dz \\
\quad = \int_{-\frac{h}{2}}^{-\frac{h_c}{2}} \frac{E_{11}(z)}{(1-\nu_{12}(z)\nu_{21}(z))}dz + \frac{E^m h_c}{(1-(\nu^m)^2)} + \int_{-\frac{h}{2}}^{\frac{h}{2}} \frac{E_{11}(z)}{(1-\nu_{12}(z)\nu_{21}(z))}dz \\
C_{22} = \int_{-\frac{h}{2}}^{-\frac{h_c}{2}} \frac{E_{22}(z)}{(1-\nu_{12}(z)\nu_{21}(z))}dz + \int_{-\frac{h_c}{2}}^{\frac{h_c}{2}} \frac{E^m}{(1-(\nu^m)^2)}dz + \int_{-\frac{h}{2}}^{\frac{h}{2}} \frac{E_{22}(z)}{(1-\nu_{12}(z)\nu_{21}(z))}dz \\
\quad = \int_{-\frac{h}{2}}^{-\frac{h_c}{2}} \frac{E_{22}(z)}{(1-\nu_{12}(z)\nu_{21}(z))}dz + \frac{E^m h_c}{(1-(\nu^m)^2)} + \int_{-\frac{h}{2}}^{\frac{h}{2}} \frac{E_{22}(z)}{(1-\nu_{12}(z)\nu_{21}(z))}dz \\
C_{12} = \int_{-\frac{h}{2}}^{-\frac{h_c}{2}} \frac{\nu_{21}(z)E_{11}(z)}{(1-\nu_{12}(z)\nu_{21}(z))}dz + \int_{-\frac{h_c}{2}}^{\frac{h_c}{2}} \frac{\nu^m E^m}{(1-(\nu^m)^2)}dz + \int_{-\frac{h}{2}}^{\frac{h}{2}} \frac{\nu_{21}(z)E_{11}(z)}{(1-\nu_{12}(z)\nu_{21}(z))}dz \\
\quad = \int_{-\frac{h}{2}}^{-\frac{h_c}{2}} \frac{\nu_{21}(z)E_{11}(z)}{(1-\nu_{12}(z)\nu_{21}(z))}dz + \frac{\nu^m E^m h_c}{(1-(\nu^m)^2)} + \int_{-\frac{h}{2}}^{\frac{h}{2}} \frac{\nu_{21}(z)E_{11}(z)}{(1-\nu_{12}(z)\nu_{21}(z))}dz \\
C_{66} = \int_{-\frac{h}{2}}^{-\frac{h_c}{2}} G_{12}(z)dz + \int_{-\frac{h_c}{2}}^{\frac{h_c}{2}} G^m dz + \int_{-\frac{h}{2}}^{\frac{h}{2}} G_{12}(z)dz \\
\quad = \int_{-\frac{h}{2}}^{-\frac{h_c}{2}} G_{12}(z)dz + G^m h_c + \int_{-\frac{h}{2}}^{\frac{h}{2}} G_{12}(z)dz\,.
\end{cases}
\tag{29}
$$

By substituting the membranes forces of Equations (24) into Equations (27), the membrane strains can be rewritten as:

$$
\begin{cases}
\varepsilon_{xx} = C_{22}^* \dfrac{\partial^2 \phi}{\partial y^2} + C_{12}^* \dfrac{\partial^2 \phi}{\partial x^2} \\
\varepsilon_{yy} = C_{12}^* \dfrac{\partial^2 \phi}{\partial y^2} + C_{11}^* \dfrac{\partial^2 \phi}{\partial x^2} \\
\gamma_{xy} = -C_{66}^* \dfrac{\partial^2 \phi}{\partial x \partial y}\,.
\end{cases}
\tag{30}
$$

By substituting Equations (30) in Equation (26), we obtain the following compatibility condition:

$$
C_{22}^* \frac{\partial^4 \phi}{\partial x^4} + (C_{66}^* + 2C_{12}^*) \frac{\partial^4 \phi}{\partial x^2 \partial y^2} + C_{11}^* \frac{\partial^4 \phi}{\partial y^4} + \frac{1}{R_1}\frac{\partial^2 w}{\partial \mathrm{x}^2} + \frac{1}{R_2}\frac{\partial^2 w}{\partial \mathrm{y}^2} = 0. \tag{31}
$$

By neglecting the shear membrane forces $N_{xy0} = 0$ and by considering the axial compression $N_{xx0} = P$ and the circumferential membrane force $N_{yy0} = 0$, the system (25)-(31) becomes:

$$\begin{cases} -D_{11}\dfrac{\partial^4 w_b}{\partial x^4} - 2(D_{12}+2D_{66})\dfrac{\partial^4 w_b}{\partial x^2 \partial y^2} - D_{22}\dfrac{\partial^4 w_b}{\partial y^4} + \dfrac{1}{R_2}\dfrac{\partial^2 \phi}{\partial y^2} + \dfrac{1}{R_1}\dfrac{\partial^2 \phi}{\partial x^2} + F\dfrac{\partial^2 w_b}{\partial x^2} - f_b = 0 \\ C_{22}^*\dfrac{\partial^4 \phi}{\partial x^4} + (C_{66}^* + 2C_{12}^*)\dfrac{\partial^4 \phi}{\partial x^2 \partial y^2} + C_{11}^*\dfrac{\partial^4 \phi}{\partial y^4} + \dfrac{1}{R_1}\dfrac{\partial^2 w}{\partial x^2} + \dfrac{1}{R_2}\dfrac{\partial^2 w}{\partial y^2} = 0. \end{cases} \quad (32)$$

3. STUDY THE BUCKLING OF THE CNT-RSSC SHELL RESTING ON ELASTIC FOUNDATION

We can solve directly the problem of the interaction between CNT-RSSC shell and an elastic foundation as an external medium. In the contact surface, the displacement at any point depends on the distribution of the pressure over the entire contact area, which causes the difficulties of the theory of elastic contact stresses. In this case the solution of an integral equation for the pressure must be found. Furthermore, the behavior of the non-elastic external environment cannot be expressed by the elasticity equations, which leads to another problem. The difficulties mentioned above can be avoided if the responses of the cylindrical shell are more interesting than the responses of the external environment. So the effect of the external medium can be expressed by relatively simple foundation models. Various foundations models are collected in Kerr model [51-52]. The design of these models is based on the replacement of an external medium by a spring interactive and dissipative elements. Springs and their shear interactions are considered in Winkler and Pasternak models. In these models, the relationship between the CNT-RSSC shell and the contact pressure can be expressed as follows:

$$\begin{cases} f = K_W w & for\ Winkler\ model \\ f = K_W w - K_G \nabla^2 w & for\ Pasterrnak\ model \end{cases} \quad (33)$$

where K_W and K_G are the spring modulus and the shear layer modulus, respectively. The term "$K_W w$" in this model assumes that the reaction force of CNT-RSSC shell is proportional to the foundation deflection at each point in the foundation which amounts to modeling the foundation by a juxtaposition of elastic springs. The second term "$K_G \nabla^2 w$" assumes that there are shear interactions between the springs [53] (see Figure 1-(b)).

Using the Equations (32) and (33), the stress functions $\phi(x,\theta)$ and the transverse displacement $w(x,\theta)$ are solutions of the equilibrium equations below:

$$\begin{cases} -D_{11}\dfrac{\partial^4 w_b}{\partial x^4} - 2(D_{12}+2D_{66})\dfrac{\partial^4 w_b}{\partial x^2 \partial y^2} - D_{22}\dfrac{\partial^4 w_b}{\partial y^4} + \dfrac{1}{R_2}\dfrac{\partial^2 \phi}{\partial y^2} + \dfrac{1}{R_1}\dfrac{\partial^2 \phi}{\partial x^2} + F\dfrac{\partial^2 w_b}{\partial x^2} \\ -K_W w + K_G \nabla^2 w = 0 \\ C_{22}^*\dfrac{\partial^4 \phi}{\partial x^4} + (C_{66}^* + 2C_{12}^*)\dfrac{\partial^4 \phi}{\partial x^2 \partial y^2} + C_{11}^*\dfrac{\partial^4 \phi}{\partial y^4} + \dfrac{1}{R_1}\dfrac{\partial^2 w}{\partial x^2} + \dfrac{1}{R_2}\dfrac{\partial^2 w}{\partial y^2} = 0\,. \end{cases} \quad (34)$$

The solution (34) can be found by searching for the solution in the following form:

$$\begin{cases} w(x,\theta) = A sin\left(\dfrac{m\pi}{a}x\right)\cos\left(\dfrac{n\pi}{b}y\right) \\ \phi(x,\theta) = a sin\left(\dfrac{m\pi}{a}x\right)\cos\left(\dfrac{n\pi}{b}y\right) \end{cases} \quad (35)$$

where A and a are arbitrary constants, n is the half wavenumber of the shell in x and m is the half wavenumber of the shell in y direction. After the substitution of the solution (35) in the problem (34), the equations of the system give:

$$\begin{cases} -D_{11}p^4A - 2(D_{12}+2D_{66})p^2q^2\mathrm{A} - D_{22}q^4\mathrm{A} + \rho_1 p^2 a + \rho_2 q^2 a + Fp^2A \\ -K_W A + K_G(p^2+q^2)A = 0 \\ C_{22}^* p^4 a + (C_{66}^* + 2C_{12}^*)p^2q^2a + C_{11}^* q^4 a + \rho_1 p^4\mathrm{A} + \rho_2 p^4 A = 0 \end{cases} \quad (36)$$

where $\rho_1 = \frac{1}{\mathrm{R}_1}$ and $\rho_2 = \frac{1}{\mathrm{R}_2}$ are the curvatures and $\mathrm{p} = \mathrm{m}\pi/\mathrm{a}$ is the wavenumber in x direction and $\mathrm{q} = \mathrm{n}\pi/\mathrm{b}$ is the wavenumber in y direction. The second equation of the system (36) leads to determine the constant a:

$$a = \frac{(\rho_1 \mathrm{p}^2 + \rho_2 \mathrm{q}^2)\mathrm{A}}{C_{22}^* \mathrm{p}^4 + (C_{66}^* + C_{12}^*)\mathrm{p}^2\mathrm{q}^2 + C_{11}^* \mathrm{q}^4}. \quad (37)$$

Replacing the above expression for a in the first equation of system (36) and I get:

$$\begin{aligned} &(-D_{11} - 2(D_{12}+2D_{66})\beta^2 - D_{22}\beta^4)p^4 + \left(F - K_G(1+\beta^2)\right)p^2 \\ &-K_w - \frac{(\rho_1 + \rho_2\beta^2)^2}{C_{22}^* + (C_{66}^* + 2C_{12}^*)\beta^2 + C_{11}^*\beta^4} = 0 \end{aligned} \quad (38)$$

where $\beta = q/p$ is the aspect ratio. Thus, we can determine the expression of the buckling load F according to β and p as follows:

$$\begin{aligned} F(\beta,p) = {} & (D_{11} + 2(D_{12}+2D_{66})\beta^2 + D_{22}\beta^4)p^2 + K_G(1+\beta^2) \\ & + \left(\frac{(\rho_1 + \rho_2\beta^2)^2}{C_{22}^* + (C_{66}^* + 2C_{12}^*)\beta^2 + C_{11}^*\beta^4} + K_w\right)\frac{1}{p^2}. \end{aligned} \quad (39)$$

The critical buckling load F_{cr} is obtained by minimizing $F(\beta,p)$ compared to the axial wave number p:

$$\left.\frac{\partial F(\beta,p)}{\partial p}\right|_{\beta\ fixed} = 0\,. \quad (40)$$

I can therefore conclude that the critical axial wave number p_{cr} is equal to :

$$p_{cr} = \left(\frac{\frac{(\rho_1+\rho_2\beta^2)^2}{C_{22}^*+(C_{66}^*+2C_{12}^*)\beta^2+C_{11}^*\beta^4} + K_w}{D_{11} + 2(D_{12}+2D_{66})\beta^2 + D_{22}\beta^4}\right)^{\frac{1}{4}}. \quad (41)$$

Finally the value of F_{cr} is calculated according to p_{cr} for a fixed aspect ratio β as follows:

$$\begin{aligned} F_{cr}(\beta) = {} & (D_{11} + 2(D_{12}+2D_{66})\beta^2 + D_{22}\beta^4)\left(\frac{\frac{(\rho_1+\rho_2\beta^2)^2}{C_{22}^*+(C_{66}^*+2C_{12}^*)\beta^2+C_{11}^*\beta^4} + K_w}{D_{11} + 2(D_{12}+2D_{66})\beta^2 + D_{22}\beta^4}\right)^{\frac{1}{2}} + \\ & \left(\frac{(\rho_1+\rho_2\beta^2)^2}{C_{22}^* + (C_{66}^*+2C_{12}^*)\beta^2 + C_{11}^*\beta^4} + K_w\right)\left(\frac{\frac{(\rho_1+\rho_2\beta^2)^2}{C_{22}^*+(C_{66}^*+2C_{12}^*)\beta^2+C_{11}^*\beta^4} + K_w}{D_{11} + 2(D_{12}+2D_{66})\beta^2 + D_{22}\beta^4}\right)^{-\frac{1}{2}} + K_G(1+\beta^2) \end{aligned} \quad (42)$$

which can be expressed as follows:

$$F_{cr}(\beta) = 2\sqrt{(D_{11} + 2(D_{12} + 2D_{66})\beta^2 + D_{22}\beta^4)\left(\frac{(\rho_1 + \rho_2\beta^2)^2}{C_{22}^* + (C_{66}^* + 2C_{12}^*)\beta^2 + C_{11}^*\beta^4} + K_w\right)} + K_G(1+\beta^2)\,. \tag{43}$$

4. NUMERICAL RESULTS

It is assumed that the core is composed of poly(methyl methacrylate) material [25-26], also called PMMA, with the properties shown in the Table 1.

Table 1. *Mechanical properties of PMMA material*

E^m(GPa)	ν^m
3.52	0.34

CNT-reinforced PMMA polymer matrix is also chosen for the matrix of the face sheets. The CNT reinforcements are chosen as (10,10) armchair single walled CNT with the material properties [28, 5455]: $E_{11}^{CN} = 5646.6\,\text{GPa}$, $E_{22}^{CN} = 7080\,\text{GPa}$, $G_{12}^{CN} = 1944.5\,\text{GPa}$ and $\nu_{12}^{CN} = 0.175$. The corrective parameters η_1, η_2 and η_3 associated to the volume fractions D_{CN}^* for CNTs-polymer composites are shown in the Table 2 [25, 26].

Table 2. *Corrective parameters* η_1, η_2 *and* η_3 *associated to the volume fractions* D_{CN}^* *for CNT-polymer composites*

D_{CN}^*	η_2	η_2	η_2
0.12	0.137	1.022	0.715
0.17	0.142	1.626	1.138
0.28	0.141	1.585	1.110

In the buckling study of CNT-RSSC shell, we compute the results by adimensional form of the critical buckling load as:

$$\bar{F} = \frac{F}{C_{110}} \tag{44}$$

and also by adimensional forms of spring constant and shear modulus as:

$$\begin{cases} \beta_W = \dfrac{K_W L^2}{C_{110}} \\ \beta_G = \dfrac{K_G}{C_{110}} \end{cases} \tag{45}$$

where C_{110} is the extension stiffness of the PMMA material given by:

$$C_{110} = \int_{-h/2}^{h/2} \frac{E^m}{(1-(\nu^m)^2)}\,dz \tag{46}$$

Thickness of the composite face sheets and the homogeneous core is respectively $h_f = 2\text{mm}$ and $h_c = 2\text{mm}$. The ratios of the radii of curvature to the thickness $\frac{R_1}{h} = \frac{R_2}{h} = 100$ and the ratios of curved edges to the thickness $\frac{a}{h} = \frac{b}{h} = 1000$.

4.1. Influence of Elastic Foundation Parameters

The effects of elastic foundation parameters, on the buckling response of the UD CNT-RSSC shell, are studied with $D^{*}_{CN} = 0.12$. For this purpose, three different stiffnesses $(\beta_W,\ \beta_G) = (0,0), (100,0), (100,0.1)$ are considered. We observe in Figure 3 that the CNT-RSSC shell without elastic foundation is less stiff than that on elastic Winkler-type foundation especially for aspect ratio values greater than 0.15 and the CNT-RSSC shell on elastic Pasternak-type foundation offers high values of stiffness. Figure 3 also shows a critical value of aspect ratio β^* equivalent to a minimum value of the critical load, the rigidity of CNT-RSSC shell increases if this critical value is avoided. Note that $\beta^* = 0.7$ and $\beta^* = 0.43$ for the Winkler and Pasternak foundations, respectively.

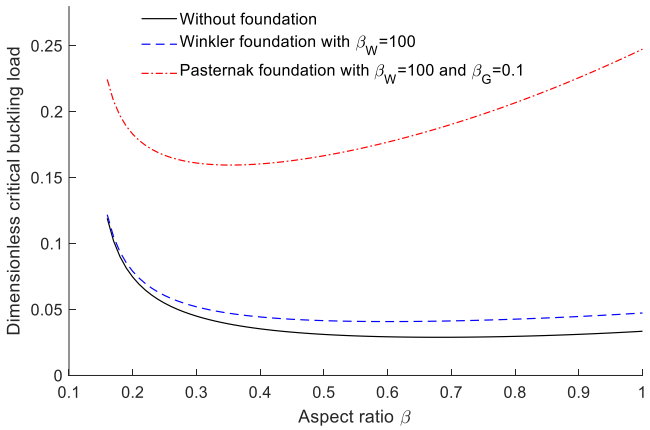

Figure 3. *Dimensionless critical buckling load* $\bar{F}$ *of CNT-RSSC shell versus aspect ratio* β *for Winkler and Pasternak models*

Figure 4 illustrates the effect of foundation stiffness on the stability of CNT-RSSC shells with UD-CNT reinforced face sheets. This figure shows that the critical buckling load increases with increasing spring stiffness or shear layer stiffness. The introduction of the Winkler or Pasternak foundation increases the stiffness of the shell

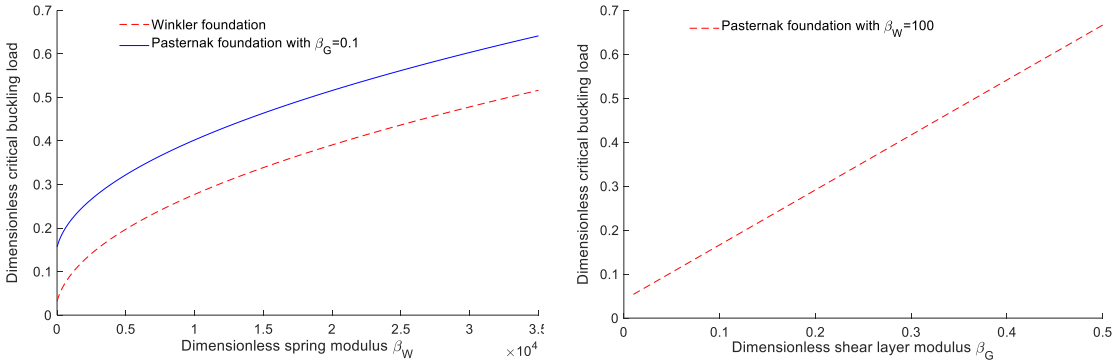

(a) : $\bar{F}$ *versus* β_W *for Winkler and Pasternak foundations*

(b) : $\bar{F}$ *versus* β_G *for Pasternak foundation*

Figure 4. *Dimensionless critical buckling load* $\bar{F}$ *of CNT-RSSC shell versus dimensionless moduli of elastic foundations*

4.2. Influence of Dispersion of CNTs and Their Volume Fraction

In Table 3, I present the dimensionless critical buckling load $(\bar{F})$ against the CNT volume fraction (D^{*}_{CN}) for different distribution profiles of CNTs. The results for the uniform and FG distributions show that $\bar{F}$ increases with increasing volume fraction D^{*}_{CN}, which shows a good correlation between the critical

buckling load and CNTs percentage. For the CNT-RSSC shell resting on elastic foundations, FG-V face sheets provide the stiffest shell, followed by the other types in the following order FG-X, UD, FG-O and FG-A. In the case without foundation, FG-X face sheets provide the stiffest shell.

Table 3. *Influence of dispersion of CNTs and their volume fraction in face sheets on dimensionless critical buckling load*

(β_W, β_G)	D^*_{CN}	UD	FG-V	FG-A	FG-X	FG-O
(0.0, 0.0)	0.12	0.0311	0.0423	0.0149	0.0388	0.0214
	0.17	0.0446	0.0621	0.0207	0.0564	0.0303
	0.28	0.0591	0.0591	0.0281	0.0772	0.0392
(100, 0.0)	0.12	0.0416	0.0555	0.0206	0.0514	0.0288
	0.17	0.0556	0.0757	0.0268	0.0694	0.0381
	0.28	0.0723	0.1029	0.0351	0.0925	0.486
(100, 0.1)	0.12	0.1666	0.1805	0.1456	0.1764	0.1538
	0.17	0.1806	0.2007	0.1518	0.1944	0.1631
	0.28	0.1973	0.2279	0.1601	0.2175	0.1736

Figure 5 demonstrates the influence of the CNT volume fraction in the face sheets on the buckling stability of CNT-RSSC shells embedded in a Pasternak foundation with stiffness $(\beta_W, \beta_G) = (100,0.1)$. The CNTs are dispersed according to the UD and FG-V patterns. I have observed that the critical buckling load increases with increasing CNT volume fraction. It is also verified that the critical buckling load $\bar{F}$ of SSC shell without reinforcement increases with increasing β and critical buckling load of CNT-RSSC shell presents a minimum against the aspect ratio β. This remark remains the same for uniform and FG distributions, but the value of β corresponding to minimum value of $\bar{F}$ depends on the dispersion of CNTs and their volume fraction in face sheets. I can conclude that there is a critical value of β which must be avoided to increase the stiffness of the shell.

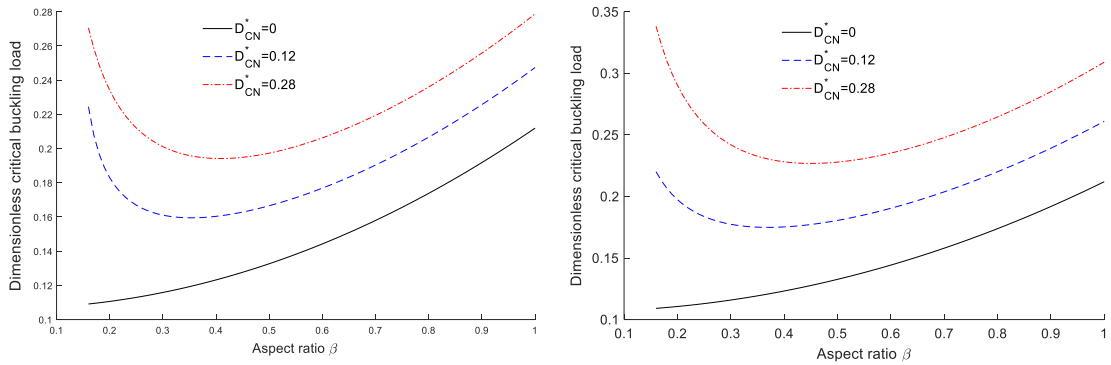

(b) : UD CNT *(b) : FG-V CNT*

Figure 5. *Influence of CNT volume fraction on stability of CNT-RSSC shell*

4.3. Effect of Geometrical Parameters

I consider that the CNT volume fraction $D^*_{CN} = 0.28$, aspect ratio $\beta = 0.5$ and a Pasternak foundation with stiffness $(\beta_W, \beta_G) = (100,0.1)$. To illustrate the influence of the thicknesses of the composite face sheet h_f and of the core h_c on the buckling stability of CNT-RSSC shell. The critical buckling load $\bar{F}$ against the thicknesses h_f and h_c are plotted in Figures 6 and 7. From these figures we observe that $\bar{F}$ decreases with increasing h_c. As h_c decreases, the difference between the results of various values of h_f becomes very small. On the other hand, $\bar{F}$ increases most rapidly with increasing h_f as shown Figures 6-(b) and 7-(b), when the value of h_f exceeds a certain value ($h_f \approx 2$mm) the increase of $\bar{F}$ slows gradually. Consequently, small core thicknesses are the best choice to improve the stiffness of CNT-RSSC shells and the optimal thickness of the composite face sheet can be used to reduce production cost of CNT-RSSC shell.

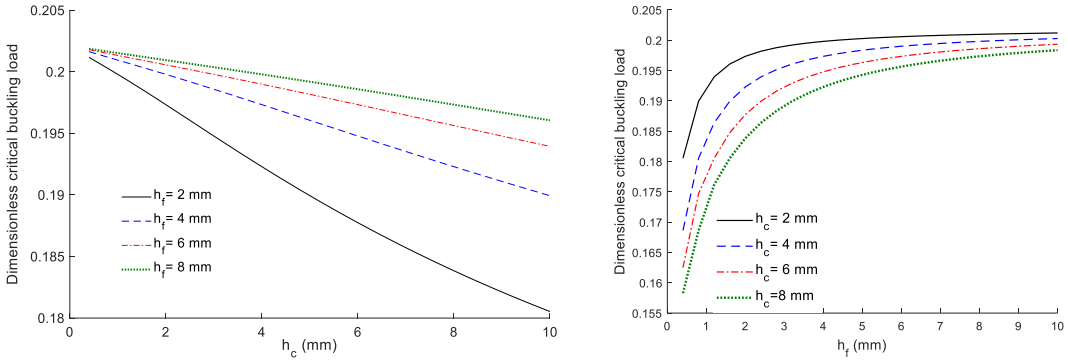

(a) : $\bar{F}$ versus h_c *(b) : $\bar{F}$ versus h_f*

Figure 6. *Buckling response of UD CNT-RSSC shell versus h_f and h_c*

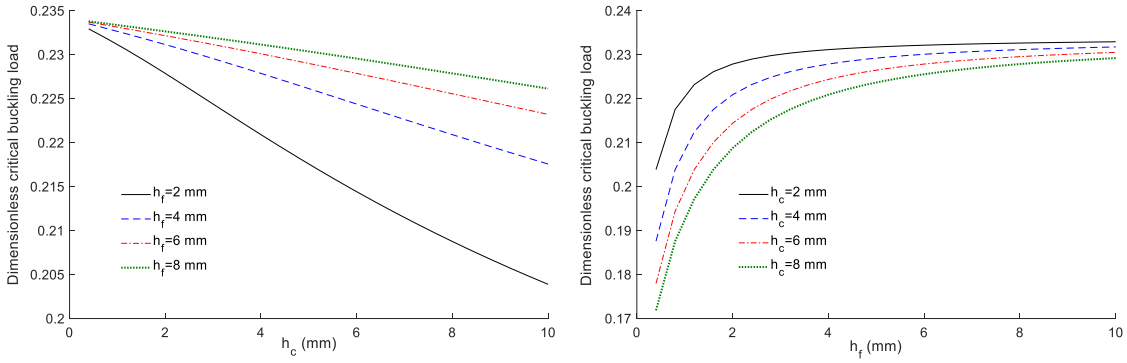

(a) : $\bar{F}$ versus h_c *(b) : $\bar{F}$ versus h_f*

Figure 7. *Buckling response of FG-V CNT-RSSC shell versus h_f and h_c*

Figure 8 shows the influence of the radius/thickness ratio (R/h) on the buckling behavior of the CNT-RSSC shell. As we can see, the load capacity of the CNT-RSSC shell decreases with increasing R/h value.

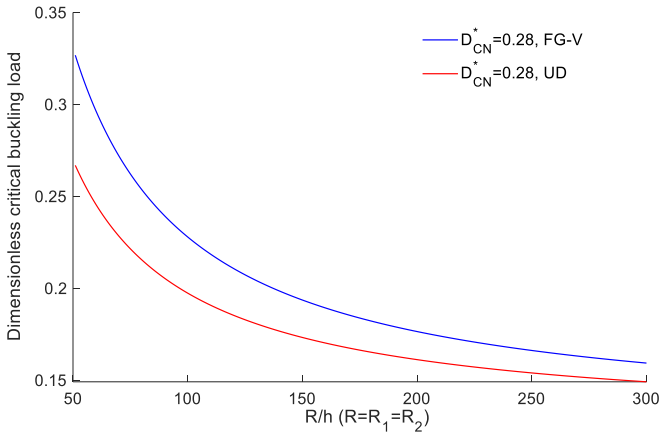

Figure 8. *Dimensionless critical buckling load $\bar{F}$ of CNT-RSSC shell versus radius/thickness ratio*

To show the effect of the geometric shape, the calculation is performed for spherical shell, cylindrical shell and flat plate by putting $R_1 = R_2 = R$, $1/R_2 \approx 0$ and $1/R_1 \approx 1/R_2 \approx 0$ in Equation (35), respectively. As shown in Figure 9, the CNT-RSSC spherical shell ($R_1 = R_2$) gives the highest stiffness values compared to the CNT-RSSC cylindrical shell ($R_2 = 10^6 h$), especially for high values of the aspect ratio, and the CNT-RSSC flat plate ($R_1 = R_2 = 10^6 h$) gives the lowest stiffness values compared to the other geometric

shapes. These results demonstrate that curvature can increase the stiffness of CNT-RSSC shell without adding thickness.

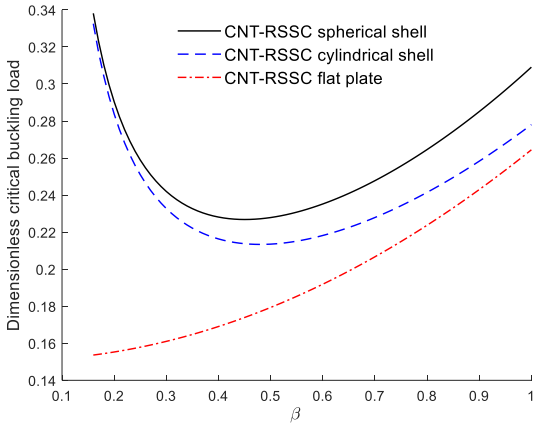

Figure 9. Effect of geometric shape on the buckling response

Further investigation on the influence of geometric shape, as shown in Table 4, reveals that critical buckling load increases with increasing volume fraction D^*_{CN} for uniform and FG distributions. The results show also that the CNT-RSSC shell with FG-A face sheets is the least stiff for the three geometric shapes. Moreover, FG-V face sheets give a higher stiffness for CNT-RSSC shells.

Table 4. *Influence of geometric shape on the dimensionless critical buckling load of the CNT-RSSC shell*

Geometric shape	D^*_{CN}	UD	FG-V	FG-A	FG-X	FG-O
Spherical shell	0.12	0.1666	0.1805	0.1456	0.1764	0.1538
	0.28	0.1973	0.2279	0.1601	0.2175	0.1736
Cylindrical shell	0.12	0.1621	0.1744	0.1436	0.1708	0.1508
	0.28	0.1880	0.2135	0.1558	0.2050	0.1676
Flat plate	0.12	0.1526	0.1610	0.1393	0.1587	0.1443
	0.28	0.1667	0.1793	0.1460	0.1759	0.1539

5. CONCLUSION

Analytical formulas are proposed for buckling analysis of CNT-RSSC shells. The effects of different parameters, such as elastic foundations, dispersion of CNTs and their volume fraction in face sheets, the core to face sheets thickness ratio, are studied with conclusions as follows:

- The CNT reinforcement of the face sheets increases the stiffness of the SSC shell.
- The CNT-RSSC shell without elastic foundation is less stiff than that on an elastic Winkler-type foundation especially for aspect ratio values greater than 0.15.
- Increasing the stiffness coefficients of the foundation causes an increase in the critical buckling loads. This is because when the stiffness coefficients of the foundation are increased, the stiffness of the CNT-RSSC shell increases.
- The CNT-RSSC shell on an elastic Pasternak-type foundation offers high values of stiffness compared to the elastic Winkler-type foundation.
- There are critical values of aspect ratio $\beta^* = 0.7$ and $\beta^* = 0.43$, for the CNT-RSSC shell embedded on Winkler and Pasternak foundations, respectively, equivalent to minimum values of critical loads. Avoiding these critical values increases the strength of the CNT-RSSC shell.
- The stiffness of the CNT-RSSC shell reduces with decrease in CNT volume fraction.
- The CNT-RSSC shell with FG-V face sheets provide the stiffest shell, followed by the other types in the following order FG-X, UD, FG-O and FG-A.
- The difference between the critical buckling loads, for several values of the face sheet thickness, becomes very small as the core thickness decreases.

- The critical buckling load rises most quickly with increasing face sheet thickness; the increase of critical buckling load slows gradually when the face sheet thickness exceeds a certain value.
- Small core thicknesses are the best choice to obtain the higher stiffness of CNT-RSSC shell and the optimal thickness of the composite face sheets reduces the production costs of the CNT-RSSC shell.
- The CNT-RSSC spherical shell gives the highest stiffness values compared to the others geometric shapes, especially for high aspect ratio values, and the CNT-RSSC flat plate gives the lowest stiffness values. Consequently, the curvature can increase the stiffness of CNT-RSSC shell without adding thickness.

I conclude that layer thicknesses, CNT volume fraction, elastic foundations parameters, geometrical parameters and the core to face sheets thickness ratio change significantly the mechanical strength of the CNT-RSSC shell. Moreover, to improve mechanical strength of CNT-RSSC shells, the volume fraction of CNTs and their dispersion in face sheets, and elastic foundations can be considered in the mechanical analysis. In the future, to improve the proposed model, the inclusion of the transverse shear strain will be considered.

CONFLICTS OF INTEREST

No conflict of interest was declared by the authors.

REFERENCES

[1] Garg, A., Aggarwal, P., Aggarwal, Y., Belarbi, M.O., Chalak, H.D., Tounsi, A., Gulia, R., "Machine learning models for predicting the compressive strength of concrete containing nano silica", Computers and Concrete, 30(1): 33-42, (2022).

[2] Bendenia, N., Zidour, M., Bousahla, A.A., Bourada, F., Tounsi, A.J., Benrahou, K.H., Adda Bedia, E.A., Mahmoud, S.R., Tounsi, A., "Deflections, stresses and free vibration studies of FG-CNT reinforced sandwich plates resting on Pasternak elastic foundation", Computers and Concrete, 26(3): 213-226, (2020).

[3] Al-Furjan, M.S.H., Hatami, A., Habibi, M., Shan, L., Tounsi, A., "On the vibrations of the imperfect sandwich higher-order disk with a lactic core using generalize differential quadrature method", Composite Structures, 257, 113150, (2021b).

[4] Huang, Y., Karami, B., Shahsavari, D., Tounsi, A., "Static stability analysis of carbon nanotube reinforced polymeric composite doubly curved micro-shell panels", Archives of Civil and Mechanical Engineering, 21:139, (2021).

[5] Heidari, F., Taheri, K., Sheybani, M., Janghorban, M., Tounsi, A., "On the mechanics of nanocomposites reinforced by wavy/defected/aggregated nanotubes", Steel and Composite Structures, 38(5): 533-545, (2021).

[6] Timesli, A., "Prediction of the critical buckling load of SWCNT reinforced concrete cylindrical shell embedded in an elastic foundation", Computers and Concrete, 26(1): 53-62, (2020).

[7] Russillo, A.F., Failla, G., Alotta, G., Sciarra, F.M., Barretta, R., "On the dynamics of nano-frames", International Journal of Engineering Science, 160, 103433, (2021).

[8] Bourada, F., Bousahla, A.A., Tounsi, A., Adda Bedia, A., Mahmoud, S.R., Benrahou, K.H., Tounsi, A., "Stability and dynamic analyses of SW-CNT reinforced concrete beam resting on elastic foundation", Computers and Concrete, 25(6), 485-495, (2020).

[9] Arshid, E., Khorasani, M., Soleimani-Javid, Z., Amir, S., Tounsi, A., "Porosity-dependent vibration analysis of FG microplates embedded by polymeric nanocomposite patches considering hygrothermal effect via an innovative plate theory", Engineering with Computers, (2021).

[10] Kong, F., Dong, F., Duan, M., Habibi, M., Safarpour, H., Tounsi, A., "On the vibrations of the Electrorheological sandwich disk with composite face sheets considering pre and pos yield regions", Thin-Walled Structures, 179, 109631, (2022).

[11] Al-Furjan, M.S.H. Habibi, M., Ghabussie, A., Safarpour, H., Safarpour, M., Tounsi, A., "Non-polynomial framework for stress and strain response of the FG-GPLRC disk using three-dimensional refined higher-order theory", Engineering Structures, 228, 111496, (2021).

[12] Al-Furjan, M.S.H., Habibi, M., Ni, J., Jung, D.W., Tounsi, A., "Frequency simulation of viscoelastic multi-phase reinforced fully symmetric systems", Engineering with Computers, (2020).

[13] Djilali, N., Bousahla, A.A., Kaci, A., Selim, M.M., Bourada, F., Tounsi, A.J., Tounsi, A., Benrahou, K.H., Mahmoud, S.R., "Large cylindrical deflection analysis of FG carbon nanotube-reinforced plates in thermal environment using a simple integral HSDT", Steel and Composite Structures, 42, 779-789, (2022).

[14] Huang, Y., Karami, B., Shahsavari, D., Tounsi, A., "Static stability analysis of carbon nanotube reinforced polymeric composite doubly curved micro-shell panels", Archives of Civil and Mechanical Engineering, 21: 139, (2021).

[15] Hajmohammad, M. H., Kolahchi, R., Zarei, M. S. and Nouri, A.H., "Dynamic response of auxetic honeycomb plates integrated with agglomerated CNT-reinforced face sheets subjected to blast load based on visco-sinusoidal theory", International Journal of Mechanical Sciences, 153-154: 391-401, (2019).

[16] Jalali, S.K. and Heshmati, M., "Buckling analysis of circular sandwich plates with tapered cores and functionally graded carbon nanotubes-reinforced composite face sheets", Thin-walled structures, 100: 14-24, (2016).

[17] Bourada, F., Bousahla, A.A., Tounsi, A., Adda Bedia, A., Mahmoud, S.R., Benrahou, K.H., Tounsi, A., "Stability and dynamic analyses of SW-CNT reinforced concrete beam resting on elastic foundation", Computers and Concrete, 25(6): 485-495, (2020).

[18] Shokravi, M., "Buckling of sandwich plates with FG-CNT-reinforced layers resting on orthotropic elastic medium using Reddy plate theory", Steel and Composite Structures, 23(6): 623-631, (2017).

[19] Shafiei, H. and Setoodeh, A.R., "Nonlinear free vibration and post-buckling of FG-CNTRC beams on nonlinear foundation", Steel and Composite Structures, 24(1): 65-77, (2017).

[20] Moradi-Dastjerdi, R. and Payganeh, G., "Transient heat transfer analysis of functionally graded CNT reinforced cylinders with various boundary conditions", Steel and Composite Structures, 24(3): 359-367, (2017).

[21] Shen, H.S., "Postbuckling of nanotube-reinforced composite cylindrical shells in thermal environments, part I: axially-loaded shells", Composite Structures, 93(8): 2096-2108, (2011).

[22] Kiani, Y., "Thermal Postbuckling of Temperature Dependent Sandwich Beams with Carbon Nanotube Reinforced Face Sheets", Journal of Thermal Stresses, 39: 1098-1110, (2016).

[23] Al-Furjan, M.S.H., Habibi, M., Jung, D.w., Sadeghi, S., Safarpour, H., Tounsi, A., Chen, G., "A computational framework for propagated waves in a sandwich doubly curved nanocomposite panel", Engineering with Computers, 38, 1679-1696 (2022).

[24] Iijima, S., "Helical microtubules of graphitic carbon", Nature, 354: 56-58, (1991).

[25] Shen, H. S., "Nonlinear bending of functionally graded carbon nanotube-reinforced composite plates in thermal environments", Composite Structures, 91(1): 9-19, (2009).

[26] Shen, H.S. and Zhang, C. L., "Thermal buckling and postbuckling behavior of functionally graded carbon nanotube-reinforced composite plates", Materials and Design, 31: 3403-3411, (2010).

[27] Sofiyev, A.H., Turkaslan, B.E., Bayramov, R.P. and Salamci, M. U., "Analytical solution of stability of FG-CNTRC conical shells under external pressures", Thin-walled Structures, 144: 106338, (2019).

[28] Mirzaei, M. and Kiani, Y., "Thermal buckling of temperature dependent FG-CNT reinforced composite conical shells", Aerospace Science and Technology, 47: 42-53, (2015).

[29] Kolahchi, R., Safari, M. and Esmailpour, M., "Dynamic stability analysis of temperature-dependent functionally graded CNT-reinforced visco-plates resting on orthotropic elastomeric medium", Composite Structures, 150: 255-265, (2016).

[30] Hajmohammad, M.H., Kolahchi, R., Zarei, M.S. and Maleki, M., "Earthquake induced dynamic detection of submerged viscoelastic cylindrical shell reinforced by agglomerated CNTs considering thermal and moisture effects", Composite Structures, 187: 498-508, (2018).

[31] Tagrara, S.H., Benachour, A., Bouiadjra, M.B. and Tounsi, A., "On bending, buckling and vibration responses of functionally graded carbon nanotube-reinforced composite beams", Steel and Composite Structures, 19: 1259-1277, (2015).

[32] Kaci, A., Tounsi, A., Bakhti, K., Adda Bedia, E.A., "Nonlinear cylindrical bending of functionally graded carbon nanotube-reinforced composite plates", Steel and Composite Structures, 12(6): 491-504, (2012).

[33] Zaitoun, M.W., Chikh, A., Tounsi, A., Al-Osta, M.A., Sharif, A., Al-Dulaijan, S.U., Al-Zahrani, M.M., "Influence of the visco-Pasternak foundation parameters on the buckling behavior of a sandwich functional graded ceramic–metal plate in a hygrothermal environment", Thin-walled Structures, 170: 108549, (2022).

[34] Mudhaffar, I.M., Tounsi, A., Chikh, A., Al-Osta, M.A., Al-Zahrani, M.M., Al-Dulaijan, S.U., "Hygro-thermo-mechanical bending behavior of advanced functionally graded ceramic metal plate resting on a viscoelastic foundation", Structures, 33: 2177-2189, (2021).

[35] Merazka, B., Bouhadra, A., Menasria, A., Selim, M.M., Bousahla, A.A., Bourada, F., Tounsi, A., Benrahou, K.H., Tounsi, A., Al-Zahrani, M.M., "Hygro-thermo-mechanical bending response of FG plates resting on elastic foundations", Steel and Composite Structures, 39(5): 631-643, (2021).

[36] Guellil, M., Saidi, H., Bourada, F., Bousahla, A.A., Tounsi, A., Al-Zahrani, M.M., Hussain, M., Mahmoud, S.R., "Influences of porosity distributions and boundary conditions on mechanical bending response of functionally graded plates resting on Pasternak foundation", Steel and Composite Structures, 38(1): 1-15, (2021).

[37] Wang, M., Li, Z.M. and Qiao, P., "Vibration analysis of sandwich plates with carbon nanotube-reinforced composite face-sheets", Composite Structures, 200: 799-809, (2018).

[38] Safaei, B., Dastjerdi, R.M., Qin, Z. and Chu, F., "Effect of thermal gradient load on thermoelastic vibrational behavior of sandwich plates reinforced by carbon nanotube agglomerations", Composite Structures, 192: 28-37, (2018).

[39] Safaei, B., Dastjerdi, R.M., Qin, Z. and Chu, F., "Frequency-dependent forced vibration analysis of nanocomposite sandwich plate under thermo-mechanical loads", Composites Part B: Engineering, 161: 44-54, (2019).

[40] Mehar, K., Panda, S.K. and Mahapatra, T. R., "Thermoelastic nonlinear frequency analysis of CNT reinforced functionally graded sandwich structure", European Journal of Mechanics; A/Solids, 65: 384-396, (2017).

[41] Medani, M., Benahmed, A., Zidour, M., Heireche, H., Tounsi, A., Bousahla, A.A., Tounsi, A.J. and Mahmoud, S.R., "Static and dynamic behavior of (FG-CNT) reinforced porous sandwich plate using energy principle", Steel and Composite Structures, 32(5): 595-610, (2019).

[42] Donnell, L. H., "Stability of Thin-Walled Tubes Under Torsion", N.A.C.A. Technical Report No. 479, (1934).

[43] Timesli, A., Braikat, B., Jamal, M. and Damil, N., "Prediction of the critical buckling load of multi-walled carbon nanotubes under axial compression", Comptes Rendus Mécanique, 345: 158-168, (2017).

[44] Asghar, S., Naeem, M.N., Hussain, M.,Taj, M. and Tounsi, A., "Prediction and assessment of nonlocal natural frequencies of DWCNTs: Vibration analysis", Computers and Concrete, 25(2): 133-144, (2020).

[45] Timesli, A., "An efficient approach for prediction of the nonlocal critical buckling load of double-walled carbon nanotubes using the nonlocal Donnell shell theory", SN Applied Sciences, 2: 407, (2020).

[46] Jam, J.E., and Kiani, Y., "Buckling of pressurized functionally graded carbon nanotube reinforced conical shells", Composite Structures, 125: 586-595, (2015).

[47] Kwon, H., Bradbury, C.R., and Leparoux, M., "Fabrication of functionally graded carbon nanotube-reinforced aluminum matrix composite", Advanced Engineering Materials, 13(4): 325-329, (2011).

[48] Shen, H.S., Wang, H., and Yang, D.Q., "Vibration of thermally postbuckled sandwich plates with nanotube-reinforced composite face sheets resting on elastic foundations", International Journal of Mechanical Sciences, 124-125: 253-262, (2017)

[49] Reddy, J.N., "Mechanics of Laminated Composite Plates and Shells, Theory and Application", CRC Press, Boca Raton, (2003).

[50] Brush, D., and Almroth, B., "Buckling of Bars, Plates and Shells", in McGraw-Hill, New York, (1975).

[51] Kerr, A.D., "Elastic and viscoelastic foundation models", Journal of Applied Mechanics, 31(3): 491-498, (1964).

[52] Kerr, A.D., "A study of a new foundation model", Acta Mechanica, 1: 135-147, (1965).

[53] Timesli, A., "Analytical Modeling of Buckling Behavior of Porous FGM Cylindrical Shell Embedded within an Elastic Foundation", Gazi University Journal of Science, 35(1): 148-165, (2022).

[54] Shen, H.S. and Xiang, Y., "Nonlinear analysis of nanotube-reinforced composite beams resting on elastic foundations in thermal environments", Engineering Structures, 56: 698-708, (2013).

[55] Manh, D.T., Anh, V.T.T., Nguyen, P.D. and Duc, N.D., "Nonlinear Post-Buckling of CNTs Reinforced Sandwich-Structured Composite Annular Spherical Shells", International Journal of Structural Stability and Dynamics, 20(2): 2050018, (2020).